

Electrochemical Synthesis of Mg-doped ZnO Nanotapers as Photocatalyst for Degradation of Bisphenol under Solar Light Irradiation

Min Wang¹, Shaochun Yuan^{1,2,*}, Bo Lv^{2,*}, Huaxian Yang³

¹ School of River and Ocean Engineering, Chongqing Jiaotong University, Chongqing, 400074, PR China

² Engineering Research Center for Sponge City Construction of Chongqing, Chongqing, 400020, PR China

³ Southwest Municipal Engineering Design & Research Institute of China, Chengdu, 610081, PR China

*E-mail: yuanse@cqjtu.edu.cn(Shaochun Yuan) and haimiancq@163.com(Bo Lv)

Received: 23 October 2020/ Accepted: 19 December 2020 / Published: 31 December 2020

This paper released electrochemical synthesis of Mg doped ZnO nanotapers for degradation of bisphenol A (BPA) as toxic aquatic pollutant under UV and visible light irradiations. The pure and Mg-doped ZnO nanotapers photo-catalysts were prepared through an electrical field assisted method. The morphological, structural and optical properties of samples were characterized through the SEM, XRD and UV-Vis absorption spectra, respectively. The morphological and structural studies exhibited that the high density of pure and doped ZnO nanostructures were grown in vertically aligned taper-like shape and hexagonal wurtzite structures. Moreover, the doping process led to creation of the cubic MgO structure in ZnO nanotaper with (111) and (220) planes. The optical characterizations showed that the higher absorption peak was observed for doped samples due to the creation of oxygen deficiency and defects in grain structure of film. The E_g values were obtained 3.48 eV and 3.09 eV for pure ZnO and Mg-doped ZnO nanotapers films, respectively. The electrochemical studies by CV and EIS techniques showed the improvement of specific capacitance of electric double layer and film's conductivity by Mg doping into ZnO matrix. The photocatalytic measurements displayed that the PBA degradation efficiencies were of 64.19 % and 100% for pure ZnO and Mg-doped ZnO nanotaper photo-catalysts for 70 minutes under UV irradiation, respectively. Therefore, the degradation efficiency of ZnO nanotapers was significantly improved by Mg doping. Furthermore, the PBA degradation efficiencies were 43.40 % and 100 % for pure and doped samples after 60 minutes under visible irradiation which indicates promotion of the degradation rate for Mg-doped ZnO nanotapers in visible irradiation. E_g value was decreased for doped samples due to the presence of Mg^{2+} inside the Zn^{2+} sites of the ZnO lattice which improve the charge separation. As a result, Mg-doped ZnO nanotapers film not only photo-excited in the UV region but also its photocatalytic activity was delayed in the visible region.

Keywords: Mg-doped ZnO nanotapers; Electrochemical technique; Photocatalyst; Bisphenol A; Photo-degradation

1. INTRODUCTION

Bisphenol A (BPA, $(\text{CH}_3)_2\text{C}(\text{C}_6\text{H}_4\text{OH})_2$) is a colorless solid organic compound of diphenylmethane derivatives that it is applied as an important precursor to make of epoxy resins, polycarbonates, polysulfones and plastics. Among them, most applicants are related to BPA-based epoxy resins and plastics. BPA-based epoxy resins are applied to preparation of thermal paper, line water pipes and food and beverage cans. BPA-based plastics are well-known for transparent and tough plastics which are used to prepare water bottles, food storage containers, baby bottles, sports equipment, CDs, and DVDs [1-3]. The huge application of BPA in food and paper industries makes it one of the highest volume of chemicals produced worldwide.

Studies showed that BPA may bind to the nuclear estrogen and androgen receptors and can reproduce the estrogen and androgen actions which affect Leydig cell steroidogenesis at high concentrations of BPA [4]. Accordingly, the European Chemicals Agency (ECHA) deduced that BPA should be considered as a substance of very high concern because of its influences on endocrine disruptor [5, 6]. Moreover, the United States Food and Drug Administration (FDA) prohibited the application of BPA in preparation of baby bottles [7].

On the other hand, environmental effects of released BPA from plastics, coat and staining manufacturers, irrigation pipes used in agriculture and wastewater of plastic, paper, and metal industries show pervasiveness of BPA makes it an important pollutant of soil and water. Several studies show at low levels BPA can harm fish and aquatic organisms [8]. Therefore, it's widely spread raises concerns and led to the start of investigations for its detection, safety and removal techniques [9-12].

Studies exhibit that ultrafiltration, coagulation, electroflotation, ozonation electrocoagulation, electrolysis, electrochemical oxidation and reduction, and photo-catalysts are the effective techniques to remove the toxic pollution from wastewaters. Among these techniques, photocatalytic degradation is an efficient procedure to remove toxic aquatic pollutants under UV and solar light irradiations on photocatalyst surfaces. Garg et al. [13] studied the photocatalytic degradation of BPA using N, Co codoped TiO_2 catalyst under sunlight and showed that 1.5% Co and 0.5% N-codoped TiO_2 samples exhibited higher photocatalytic activity than commercial TiO_2 . Kuo et al. [14] evaluated the photodegradation performance of BPA in a visible light on TiO_2 /polyethyleneglycol photocatalyst. Their results showed adding polyethylene glycol to TiO_2 structure enhanced the photoactivity.

To the best of our knowledge, this is the first study to synthesize taper-like Mg-doped ZnO nanostructures on indium tin oxide glass by a facile electrochemical technique for degradation of BPA as toxic aquatic pollutant under UV and visible light irradiations.

2. MATERIALS and METHOD

Mg-doped ZnO nanopapers were synthesized through electrochemical technique. The solution was prepared from the mixture of 0.4 M zinc acetate dihydrate (99 %, Lianyungang Zhonghong Chemical Co., Ltd., China) as precursor solution, 0.2 M acetic acid (Shijiazhuang Xinlongwei Chemical Co., Ltd., China) and 0.15 M toluene (> 85%, Shandong S-Sailing Chemical Co., Ltd., China) as catalysts in volume ratio of 2:1:1[15, 16]. Then, 0.1 M magnesium sulfate (99.5%, Zhong Tang (Dalian) Materials Co., Ltd., China) as dopant source was added to the mixture in volume ratio of 1:2 and the final mixture was stirred for 15 minutes to obtain the homogenous transparent solution. The indium tin oxide glass (ITO, Merck, Germany) as working electrode and graphite bar (length of 10 cm, Tianjin Dashi Carbon Co., Ltd., China) were immersed into the prepared solution of an electrochemical cell under stirring condition. The DC voltage of 0.4 V was applied between two electrodes for 60 minutes. After that, the electrode was rinsed with deionized water.

The morphology of pure ZnO and Mg-doped ZnO nanopaper photo-catalysts were studied by scanning electron microscopy (SEM, JEOL JSM-6390LV/LGS, Tokyo, Japan). The structural properties and crystal phase of the samples were characterized by X-ray diffraction (XRD, Philips PW 1050, The Netherlands) which operated at 40 kV and 30 mA in wavelength of CuK α ($\lambda=1.5418 \text{ \AA}$). The optical absorption spectra of the samples were recorded using a UV-VIS spectrophotometer (Hitachi U-2800, Tokyo, Japan). CV and EIS measurements were performed with Metrohm Autolab instruments in a standard three-electrode electrochemical cell which contained Ag/AgCl electrode as a reference electrode, Pt wire as a counter electrode and the prepared pure ZnO and Mg-doped ZnO nanopapers as working electrode. The electrolyte of CV measurements was 0.1 M phosphate buffer solution (PBS) which prepared by Na₂HPO₄ (99.0%, Hangzhou Focus Corporation, China). The electrolyte solution of EIS experiments was 0.5 M Na₂SO₄ (99%, Tianjin Wodehaotai Trading Co., Ltd., China).

The photo-catalytic experiments were conducted with initial concentration of PBA (99%, Hebei Guanlang Biotechnology Co., Ltd., China) equal to 5, 10, 20 and 50 mg l⁻¹ in presence of pure ZnO and Mg-doped ZnO nanopapers photo-catalysts. The measurements were carried out using a cylindrical photo-reactor with internal diameter of 3 cm and height of 22 cm which was irradiated with UV and visible light sources. The photo-degradation system was left in the dark for 60 minutes to establish an adsorption-desorption equilibrium between the photo-catalysts and PBA solution, and then photocatalytic reactions were performed under light irradiations. The change in PBA concentrations was analyzed with optical absorption spectra which recorded with spectrophotometer (Perkin Elmer UV-vis spectrophotometer at $\lambda=663 \text{ nm}$). The degradation efficiency (%) was calculated with recorded intensity of in optical absorption spectra of irradiated PBA as following equation [17]:

$$\text{Degradation efficiency (\%)} = \frac{I_0 - I_t}{I_0} \times 100 = \frac{C_0 - C_t}{C_0} \times 100 \quad (1)$$

Where, I_0 and I_t are the absorption intensity of PBA solution before and after photocatalytic reaction, respectively. C_0 and C_t are the concentrations of PBA before and after the photo-degradation process, respectively.

3. RESULTS and DISCUSSION

Figure 1 depicts SEM images of the synthesized pure ZnO and Mg-doped ZnO structures on the ITO substrates via electrical field assisted technique which implying the high density of pure and doped ZnO nanostructures were grown in vertically aligned taper-like shape. There are the hexagonal stems with a tapering tip for any nanotaper structure. As observed in Figure 1, average diameters of pure ZnO and Mg-doped ZnO nanotapers are estimated 170 nm and 250 nm in the middle of structures, respectively. The average lengths of nanotapers are 1.7 μm and 2.3 μm for pure ZnO and Mg-doped ZnO structures, respectively.

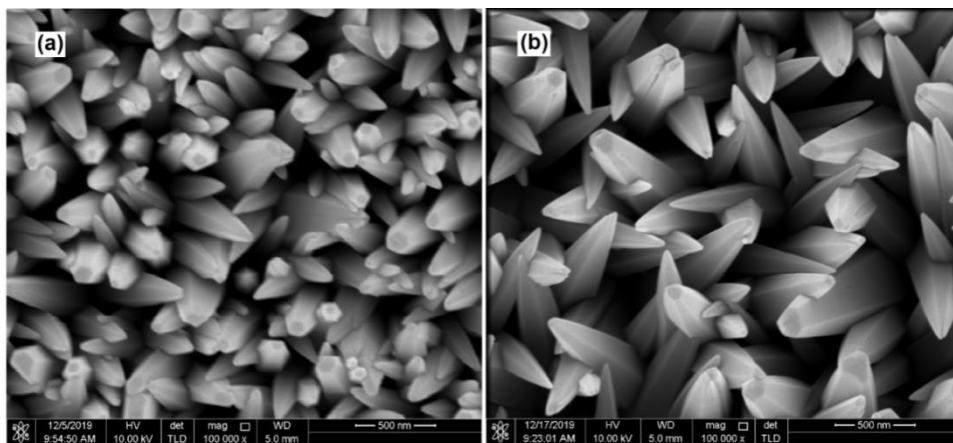


Figure 1. SEM images of the synthesized (a) pure ZnO and (b) Mg-doped ZnO nanotapers on the ITO substrates via electrical field assisted technique.

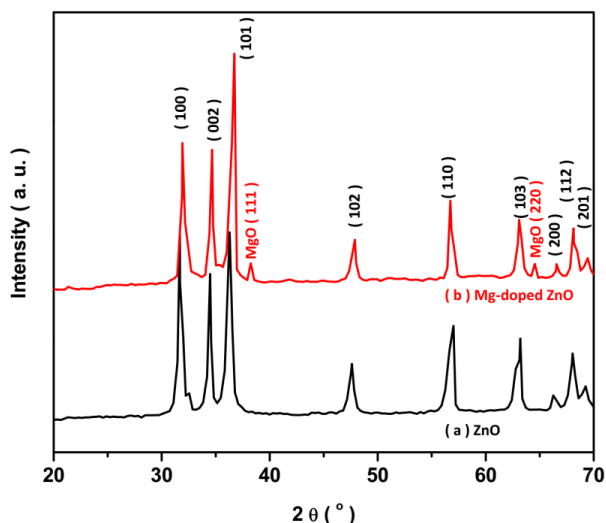


Figure 2. XRD patterns of the synthesized (a) pure ZnO and (b) Mg-doped ZnO nanotapers.

Figure 2 shows XRD patterns of the synthesized pure ZnO and Mg-doped ZnO nanotapers. The diffraction peaks at $2\theta = 31.89^\circ, 34.70^\circ, 36.77^\circ, 47.95^\circ, 56.81^\circ, 63.12^\circ, 66.89^\circ, 68.23^\circ$ and 69.44° that is corresponding to form (100), (002), (101), (102), (110), (103), (200), (112) and (201) planes (JCPDS card No. 075-1526), respectively which indicates to the growth of samples in hexagonal wurtzite

structures [18, 19]. Furthermore, XRD pattern of Mg-doped ZnO displays two diffraction peaks at $2\theta = 37.94^\circ$ and 63.87° which relate to the formation of the cubic MgO structure in doped samples with (111) and (220) planes (JCPDS card No. 45-0946) [20, 21], respectively.

Figure 3a shows the recorded CVs of pure ZnO and Mg-doped ZnO nanotapers films in 0.1 M PBS solution pH 6 at scan rate of 10 mVs^{-1} with potential range of -0.1 to 0.8 V. As seen, Mg-doped ZnO film shows larger surrounded area of the CV which demonstrates the improvement of specific capacitance of electric double layer due to the doping Mg ion into the ZnO lattice [22]. It can enhance the charge storage value and better electronic storage capability of Mg-doped ZnO film toward pure ZnO film. EIS measurements were carried out to prepare films with frequency range of 10^{-1} to 10^5 Hz at applied voltage of 5 mV in 0.5 M Na_2SO_4 solution. Figure 3b shows the Nyquist plots of the samples that was obviously indicated the smaller resistance of the doped film than pure ZnO film, which refer to improvement of the film's conductivity by doping Mg ions into ZnO film due to the synergistic effect between ZnO and Mg nanostructures [23, 24]. Furthermore, high electron transfer rate can be related to more interfaces between ZnO and Mg [25].

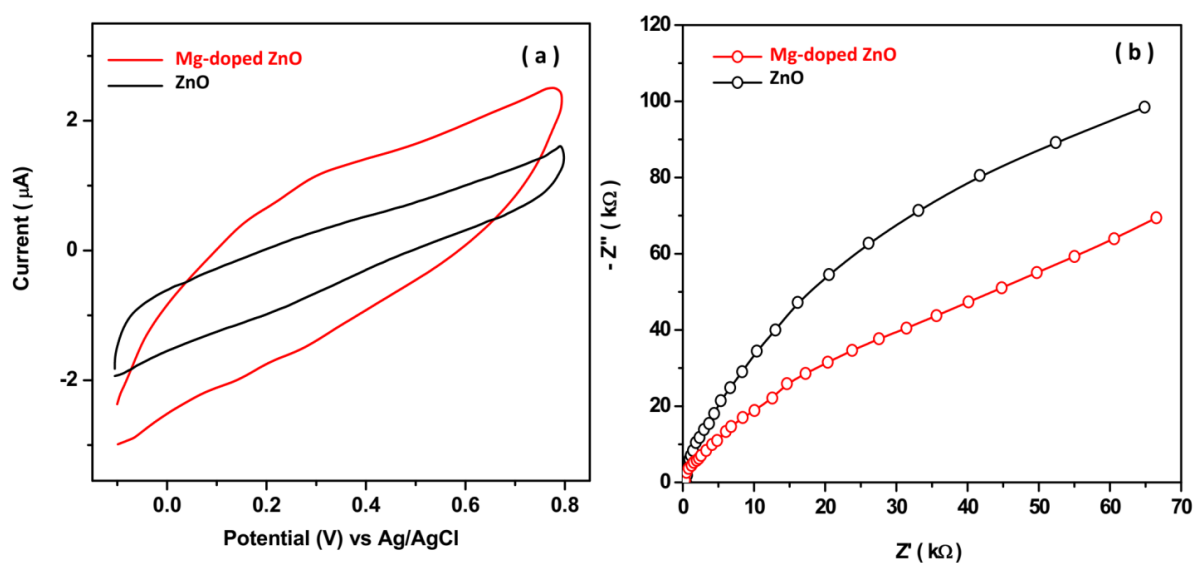


Figure 3. (a) The recorded CVs of pure ZnO and Mg-doped ZnO nanotapers films in 0.1 M PBS solution pH 6 at scan rate of 10 mVs^{-1} with potential range of -0.1 to 0.8 V. (b) The Nyquist plots of EIS measurements of pure ZnO and Mg-doped ZnO nanotapers films with frequency range of 10^{-1} to 10^5 Hz at applied 5 mV AC voltage in 0.5 M Na_2SO_4 solution.

Figure 4 shows the recorded UV-Vis absorption spectra of pure ZnO and Mg-doped ZnO nanotapers films at wavelength range of 220 to 1100 nm. As shown, the higher absorption peak belongs to doped samples which may be due to the creation of oxygen deficiency and defects in grain structure of film [26]. The sharp absorbance peak was observed at wavelength of 370 nm and 380 nm for pure ZnO and Mg-doped ZnO films, respectively which indicates a redshift in the absorption edge of doped film due to the Mg doping into the ZnO lattice and generation of a small amount of lattice strain in the doped film [27, 28]. This redshift can be attributed to the reduction of the Fermi level of doped ZnO film by formation of intragap states which can modify the absorption of the ZnO film in visible

regions [29, 30]. The optical bandgap energy (E_g) of the samples are obtained through Tauc equation (2) [31]:

$$\alpha h\nu = A(h\nu - E_g)^n \quad (2)$$

Where α is absorption coefficient, h is Planck's constant (4.1357×10^{-15} eV s), ν is the frequency of irradiated light and n value is $\frac{1}{2}$ that means allowed direct transition [32]. Figure 4b shows the Tauc plots ($(\alpha h\nu)^2$ versus $(h\nu)$) of samples that the E_g are determined from extrapolation of the linear fits of the Tauc plots onto the x -axis [32]. The E_g values were obtained 3.48 eV and 3.09 eV for pure ZnO and Mg-doped ZnO nanopapers, respectively. Accordingly, E_g value was decreased for doped samples due to the presence of Mg^{2+} inside the Zn^{2+} sites of the ZnO lattice [33]. Moreover, the decrease in E_g value may be associated with the increment of localized state density in the conduction band of ZnO [34]. Therefore, optical results show that the Mg-doped ZnO nanopapers film not only photoexcited in the UV region but also its photocatalytic activity is expanded in the visible region.

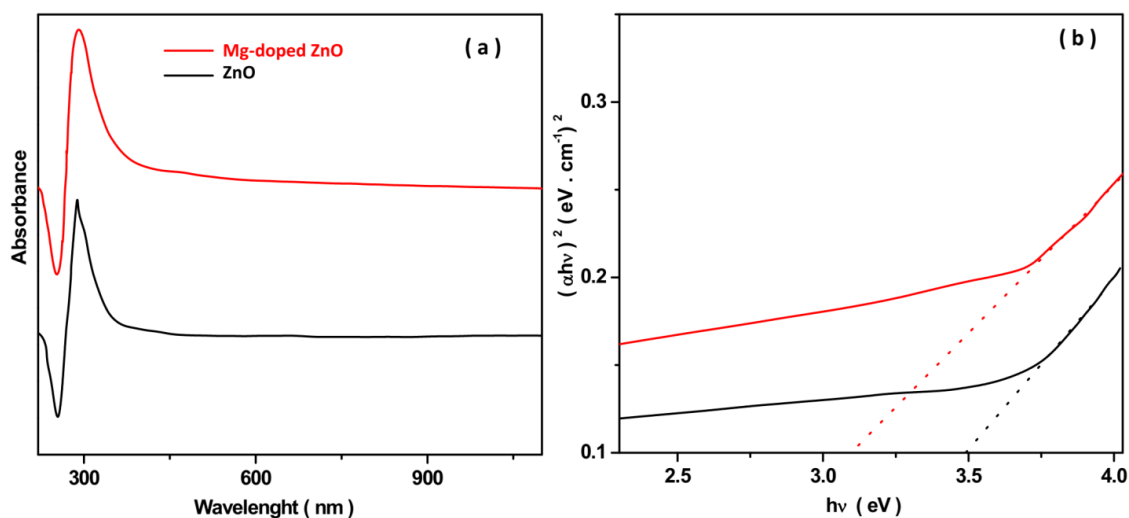


Figure 4. (a) The recorded absorption spectra and (b) Tauc plots of pure ZnO and Mg-doped ZnO nanopapers films.

Figure 5a shows the degradation efficiency of 10 mg l^{-1} PBA in the presence of pure ZnO and Mg-doped ZnO nanopapers photocatalysts and without photocatalyst (blank) under dark and UV irradiations. As shown, the degradation efficiencies of 0.32 %, 2.09 % and 3.19 % were obtained for blank, pure ZnO and Mg-doped ZnO nanopapers photocatalysts for 30 minutes under dark conditions, respectively. Moreover, the PBA degradation efficiencies were 1.85 %, 64.19 % and 100% for the blank sample, pure ZnO and Mg-doped ZnO nanopapers photocatalysts for 70 minutes UV irradiation, respectively. Thus, the degradation efficiency of ZnO nanopapers was significantly enhanced by Mg doping. Figure 5b shows the photo-degradation activity of prepared photocatalysts under visible irradiation that indicates the PBA degradation efficiencies were 43.40 % and 100 % for pure and doped samples after 60 minutes under visible irradiation. Therefore, the comparison between results of figure 5a and 5b is demonstrated that degradation rate is promoted for Mg-doped ZnO nanopapers in visible

irradiation. This can be related to the reduction of E_g value and change of optical properties on doped photo-catalyst [35-37]. Furthermore, Mg doping can improve the charge separation due to the creation of physical defects as oxidation states which can act as similar to sink for trapping sites for the photogenerated holes and electrons and impede their recombination rate [38, 39].

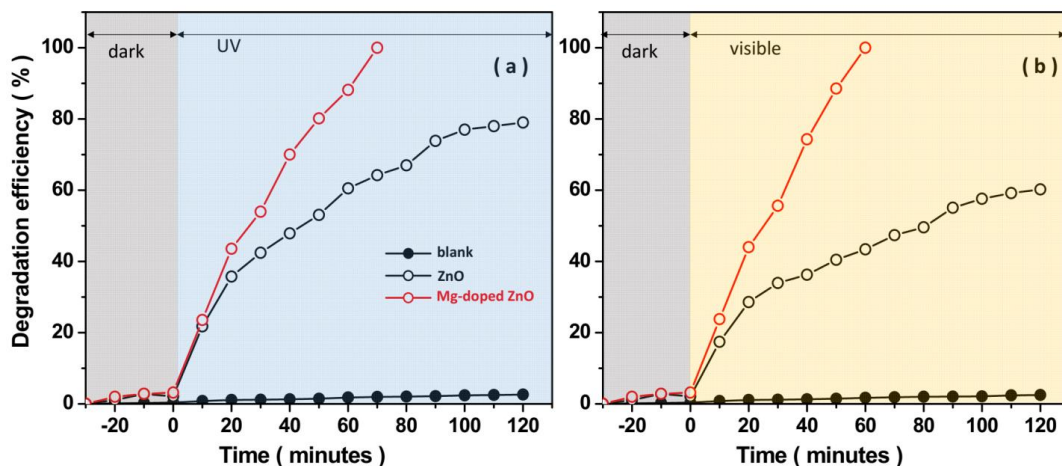


Figure 5. Degradation efficiency of 10 mg l^{-1} PBA in present of pure ZnO and Mg-doped ZnO nanotapers photo-catalysts and blank sample under dark condition and irradiation (a) UV and (b) visible light.

Figures 6a and 6b show the PBA degradation efficiency on Mg-doped ZnO nanotapers photocatalyst surface for various PBA concentrations under UV and visible irradiations, respectively. As shown, the rate of photodegradation in visible irradiation was more than UV irradiation. The 100% degradation of 5, 10, 20 and 50 mg l^{-1} of BPA occur after 60, 70, 130 and 180 minutes under UV irradiation, respectively. Moreover, complete degradation for 5, 10, 20 and 50 mg l^{-1} of BPA were observed after 50, 60, 120 and 170 minutes under visible irradiation. Table 1 displays a comparison between the degradation efficiency of this photocatalyst and Cu-deposited N TiO₂/titanate nanotubes [40], TiO₂ [41], Ag-TiO₂ [42], Bi₂WO₆/CoFe₂O₄ [43], C-ZnO [44] for BPA degradation. As observed, the synthesized Mg-doped ZnO nanotapers photocatalyst exhibited better photocatalytic performance for 5, 10, 20 and 50 mg l^{-1} degradation of BPA under both UV and visible irradiations. The Mg-doped ZnO nanotapers can excite upon visible light and the photoexcited carrier of conduction and valence bands of the doped ZnO nanotapers can react with H₂O/OH⁻ and O₂ molecules on the surface of photocatalyst and induce active species such as [•]OH and O₂^{-•} radicals [45, 46].

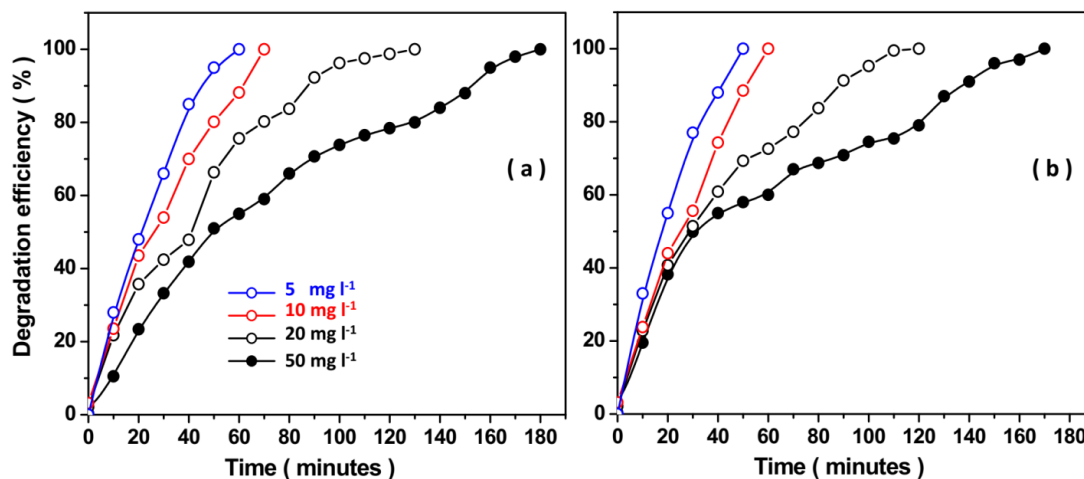


Figure7. PBA degradation efficiency on Mg-doped ZnO nanopapers photocatalyst surface for various PBA concentrations under (a) UV and (b) visible irradiations.

Table 1. Comparison between the degradation performances of Mg-doped ZnO nanopapers photocatalyst and the other reported photo-catalysts of literature for degradation of BPA.

Catalyst	BPA concentration (mg l ⁻¹)	Light source	Degradation efficiency (%)	Irradiation time (minute)	Ref.
Cu-deposited TiO ₂ /titanate nanotubes	5	UV	100.0	180	[40]
TiO ₂	10	UV	97.0	360	[41]
Ag-TiO ₂	10	UV	97.0	120	[42]
Bi ₂ WO ₆ /CoFe ₂ O ₄	20	Visible	92.0	120	[43]
C-ZnO	50	UV	100.0	1440	[44]
Mg-doped nanopapers	ZnO 5	UV Visible	100.0 100.0	60 50	This study
Mg-doped nanopapers	ZnO 10	UV Visible	100.0 100.0	70 60	This study
Mg-doped nanopapers	ZnO 20	UV Visible	100.0 100.0	130 120	This study
Mg-doped nanopapers	ZnO 50	UV Visible	100.0 100.0	180 170	This study

4. CONCLUSION

This study was focused on synthesis of Mg-doped ZnO nanopapers for removal of toxic aquatic pollutants under solar light irradiation. The pure and Mg-doped ZnO nanopapers photo-catalysts were synthesized through an electrical field assisted method and its physical properties were characterized through the SEM, XRD and UV-Vis absorption spectra. The SEM studies showed that the high density of pure and doped ZnO nanostructures were grown in vertically aligned taper-like shape. XRD analyses revealed that both samples were grown in hexagonal wurtzite structures and the doping process led to creation of the cubic MgO structure in ZnO nanopaper with (111) and (220) planes. The

optical studies showed that the higher absorption peak was belonging to doped samples which may be due to creation of oxygen deficiency and defects in grain structure of film. The E_g values were obtained 3.48 eV and 3.09 eV for pure ZnO and Mg-doped ZnO nanotapers films, respectively. Therefore, E_g value was decreased for doped sample due to the presence of Mg^{2+} inside the Zn^{2+} sites of the ZnO lattice which implies the Mg-doped ZnO nanotapers film not only photoexcited in UV region but also its photocatalytic activity was expanded in visible region. The electrochemical properties of the samples were studied by CV and EIS techniques which showed the improvement of specific capacitance of electric double layer and film's conductivity by Mg doping into ZnO film. The photocatalytic studies showed that the PBA degradation efficiencies were of 64.19 % and 100% for pure ZnO and Mg-doped ZnO nanotapers photo-catalysts for 70 minutes under UV irradiation, respectively. Thus, the degradation efficiency of ZnO nanotapers was significantly enhanced by Mg doping. Moreover, the PBA degradation efficiencies were 43.40 % and 100 % for pure and doped samples after 60 minutes under visible irradiation. Therefore, the degradation rate was promoted for Mg-doped ZnO nanotapers in visible irradiation. This can be related to the reduction of E_g value and change of optical properties on doped photocatalyst. Furthermore, Mg doping can improve the charge separation due to the creation of physical defects as oxidation states which can act as similar to sink for trapping sites of the photogenerated holes and electrons and delay their recombination rate.

ACKNOWLEDGEMENT

The authors are grateful for the financial support provided by the Natural Science Foundation of Chongqing (cstc2020jcyj-msxmX1000) and Chongqing Construction Technology Plan Project (2020-5-7).

References

1. R. Bashiri, N.M. Mohamed, C. F. Kait, S. Sufian, S. Kakooei, M. Khatani, Z. Gholami, *Renewable Energy*, 99(2016)960.
2. H. Karimi-Maleh and O.A. Arotiba, *Journal of colloid and interface science*, 560(2020)208.
3. J. Rouhi, S. Mahmud, S.D. Hutagalung and S. Kakooei, *Journal of Micro/Nanolithography, MEMS, and MOEMS*, 10(2011)043002.
4. O. Keminer, M. Teigeler, M. Kohler, A. Wenzel, J. Arning, F. Kaßner, B. Windshügel and E. Eilebrecht, *Science of The Total Environment*, 717(2020)134743.
5. L. Trasande, R.T. Zoeller, U. Hass, A. Kortenkamp, P. Grandjean, J.P. Myers, J. DiGangi, M. Bellanger, R. Hauser and J. Legler, *The Journal of Clinical Endocrinology & Metabolism*, 100(2015)1245.
6. M. Miraki, H. Karimi-Maleh, M.A. Taher, S. Cheraghi, F. Karimi, S. Agarwal and V.K. Gupta, *Journal of Molecular Liquids*, 278(2019)672.
7. K. Aschberger, P. Castello, E. Hoekstra, S. Karakitsios, S. Munn, S. Pakalin and D. Sarigiannis, *Luxembourg: Publications Office of the European Union*, 10(2010)5.
8. J.H. Kang, D. Aasi and Y. Katayama, *Critical reviews in toxicology*, 37(2007)607.
9. B. Ntsendwana, B. Mamba, S. Sampath and O. Arotiba, *International Journal of Electrochemical Science*, 7(2012)3501.
10. L. Gui, H. Jin, Y. Zheng, R. Peng, Y. Luo and P. Yu, *International Journal of Electrochemical Science*, 13(2018)7141.
11. Q. Li, T. Li and Q. Wang, *International Journal of Electrochemical Science*, 15(2020)6759.

12. H. Karimi-Maleh, C.T. Fakude, N. Mabuba, G.M. Peleyeju and O.A. Arotiba, *Journal of colloid and interface science*, 554(2019)603.
13. A. Garg, T. Singhania, A. Singh, S. Sharma, S. Rani, A. Neogy, S.R. Yadav, V.K. Sangal and N. Garg, *Scientific reports*, 9(2019)1.
14. C.Y. Kuo, C.H. Wu and H.Y. Lin, *Desalination*, 256(2010)37.
15. C. Dwivedi and V. Dutta, *Applied Physics A*, 109(2012)75.
16. Z. Liu, R. Zhu and G. Zhang, *Journal of Physics D: Applied Physics*, 43(2010)155402.
17. G. Safari, M. Hoseini, M. Seyedsalehi, H. Kamani, J. Jaafari and A. Mahvi, *International Journal of Environmental Science and Technology*, 12(2015)603.
18. H. Savaloni and R. Savari, *Materials Chemistry and Physics*, 214(2018)402.
19. J. Rouhi, C.R. Ooi, S. Mahmud and M.R. Mahmood, *Electronic Materials Letters*, 11(2015)957.
20. L.Z. Pei, W.Y. Yin, J.F. Wang, J. Chen, C.G. Fan and Q.F. Zhang, *Materials Research*, 13(2010)339.
21. R. Dalvand, S. Mahmud, J. Rouhi and C.R. Ooi, *Materials Letters*, 146(2015)65.
22. X. Xiao, B. Han, G. Chen, L. Wang and Y. Wang, *Scientific reports*, 7(2017)1.
23. C.F. Lin, C.H. Kao, C.Y. Lin, Y.W. Liu and C.H. Wang, *Results in Physics*, 16(2020)102976.
24. H. Karimi-Maleh, K. Cellat, K. Arıkan, A. Savk, F. Karimi and F. Şen, *Materials Chemistry and Physics*, 250(2020)123042.
25. M.M. Tavakoli, R. Tavakoli, P. Yadav and J. Kong, *Journal of Materials Chemistry A*, 7(2019)679.
26. F.A. Mir and K.M. Batoo, *Applied Physics A*, 122(2016)418.
27. D. Arora, K. Asokan, A. Mahajan, H. Kaur and D. Singh, *RSC advances*, 6(2016)78122.
28. F. Tahernejad-Javazmi, M. Shabani-Nooshabadi and H. Karimi-Maleh, *Composites Part B: Engineering*, 172(2019)666.
29. W. Vallejo, A. Cantillo and C. Díaz-Uribe, *International Journal of Photoenergy*, 2020(2020)1.
30. R. Mohamed, J. Rouhi, M.F. Malek and A.S. Ismail, *International Journal of Electrochemical Science*, 11(2016)2197.
31. N.N. Ilkhechi, M. Alijani and B.K. Kaleji, *Optical and quantum electronics*, 48(2016)148.
32. M. Sharmin and A. Bhuiyan, *Journal of Materials Science: Materials in Electronics*, 30(2019)4867.
33. Z. Shamsadin-Azad, M.A. Taher, S. Cheraghi and H. Karimi-Maleh, *Journal of Food Measurement and Characterization*, 13(2019)1781.
34. M. Mozammel, N.N. Ilkhechi, E.F. Tanouraghaj and E. Rezaei, *Journal of the Australian Ceramic Society*, 55(2019)999.
35. M. Samadi, M. Zirak, A. Naseri, E. Khorashadizade and A.Z. Moshfegh, *Thin Solid Films*, 605(2016)2.
36. R. Hassanzadeh, A. Siabi-Garjan, H. Savaloni and R. Savari, *Materials Research Express*, 6(2019)106429.
37. M. Alimanesh, J. Rouhi and Z. Hassan, *Ceramics International*, 42(2016)5136.
38. L. Wang, Y. Wu, F. Chen and X. Yang, *Progress in Natural Science: Materials International*, 24(2014)6.
39. K. Sadaiyandi, A. Kennedy, S. Sagadevan, Z.Z. Chowdhury, M.R.B. Johan, F.A. Aziz, R.F. Rafique and R.T. Selvi, *Nanoscale research letters*, 13(2018)229.
40. R.A. Doong and C.Y. Liao, *Separation and Purification Technology*, 179(2017)403.
41. R. Wang, D. Ren, S. Xia, Y. Zhang and J. Zhao, *Journal of Hazardous Materials*, 169(2009)926.
42. S. Rengaraj and X.-Z. Li, *International journal of environment and pollution*, 27(2006)20.
43. C. Wang, L. Zhu, C. Chang, Y. Fu and X. Chu, *Catalysis Communications*, 37(2013)92.

44. O. Bechambi, S. Sayadi and W. Najjar, *Journal of Industrial and Engineering Chemistry*, 32(2015)201.
45. A. Phuruangrat, S. Siri, P. Wadbua, S. Thongtem and T. Thongtem, *Journal of Physics and Chemistry of Solids*, 126(2019)170.
46. S. Sa-nguanprang, A. Phuruangrat, T. Thongtem and S. Thongtem, *Russian Journal of Inorganic Chemistry*, 64(2019)1841.

© 2021 The Authors. Published by ESG (www.electrochemsci.org). This article is an open access article distributed under the terms and conditions of the Creative Commons Attribution license (<http://creativecommons.org/licenses/by/4.0/>).